JOURNAL OF SPACECRAFT AND ROCKETS
Vol. 32, No. 4, July–August 1995

Material-Property Effects on a Thin-Film Solar Concentrator

Paul A. Gierow* and James P. Paxton†
SRS Technologies, Huntsville, Alabama 35806
and
Thomas L. Cost‡ and Clark W. Hawk§
University of Alabama in Huntsville, Huntsville, Alabama 35899

The successful implementation of solar thermal propulsion is dependent upon the use of a deployable concentrator. One approach to concentrator design is that of a concentrator supported by an inflatable torus. This concentrator is made of a castable thin-film polyimide that has an elliptical reflective portion that concentrates the sun's energy to a focal point at the rocket's absorber. The effects of thin-film material properties and varied environmental conditions upon the final focal point of such a concentrator were evaluated by comparative analysis. The material properties varied include modulus of elasticity, coefficient of thermal expansion, coefficient of moisture expansion, and Poisson's ratio. The environmental conditions varied were temperature and humidity. In addition, concentrator design parameters of film thickness and applied pressure were also varied. The changes in concentrator geometry due to an applied pressure, film thickness, and environmental conditions were predicted using a computer code written specifically for this purpose. The deflected shape was then used in an optical ray-trace code to determine the optimum focal length and the focal-point distribution. Film thickness and inflation pressure were found to have the greatest effect on focal-point dispersion.

Nomenclature

CME = coefficient of moisture expansion, in./(in. %RH)
CTE = coefficient of thermal expansion, in./(in. °F)
E = modulus of elasticity, psi
f = fixed focal length measured from vertex of membrane, in.
f_o = optimum focal length measured from vertex of membrane, in.
$f_o - f$ = focal-length increase, in.
Offset = horizontal shift at center of membrane, in.
P = applied pressure, psi
rms = scatter of rays at focal point of reflector, in.
T_f = film thickness at edge of membrane, in.
T_i = film thickness at center of membrane, in.
ΔRH = change in relative humidity, %
ΔT = change in temperature, °F
ν = Poisson's ratio, in./in.

Introduction and Background

SOLAR thermal propulsion (STP) is attracting increasing interest as an option for upper-stage rocket design. As presently envisioned, a typical solar-powered rocket, shown in Fig. 1, contains a deployable solar concentrator, a concentrator support structure, and an absorber. The concentrator collects the sun's energy and focuses it to a point on the absorber. The absorber is heated by the concentrated energy and transfers this heat energy to hydrogen, which cools the absorber. The high-temperature hydrogen gas is passed through a nozzle, where the gas acceleration produces thrust to propel the rocket. STP systems provide typical I_{sp} values ranging from 600 to 1000 s at thrust levels of 1 to 2 lbf, which in turn offer weight advantages over higher-power chemical-rocket-powered upper stages. The concept of STP was developed for such applications as satellite orbit circularization and on-orbit satellite maneuvers.

Received Aug. 5, 1994; presented as Paper 94-3029 at the AIAA/ASME/SAE/ASEE 30th Joint Propulsion Conference; revision received March 13, 1995; accepted for publication March 13, 1995.

*Principal Engineer.
†Senior, Mechanical Engineering. Member AIAA.
‡Professor, Mechanical and Aerospace Engineering. Associate Fellow AIAA.
§Professor, Mechanical and Aerospace Engineering; Director, Propulsion Research Center. Associate Fellow AIAA.

As shown in Fig. 1, the propulsion system will contain two concentrators, one on either side of the absorber/thruster. The mirrors in this application are estimated to be 15–75 ft in diameter, depending upon the thrust levels. Because of the size of these reflectors, their design must permit them to be collapsed initially to be stowable within the payload shroud. Additionally, the reflectors must be light to minimize the weight of the propulsion system. A concentrator system[1] has been proposed to meet these criteria and is presented conceptually in Fig. 2. This concentrator will be constructed of a thin-film polyimide material. It will contain a reflective portion, having a parabolic shape, which will act as the concentrator, and a transparent portion to form the pressurized chamber and permit the passage of the light rays. The concentrators will be stowed in the payload shroud and deployed by inflation of the volume between the reflectorized and transparent walls when the spacecraft is in Earth orbit. The concentrator assembly is held in place by a self-rigidizing support structure.[1]

The success of any concentrator design depends upon the accuracy of the reflector. The reflector's focus must be optimized, and

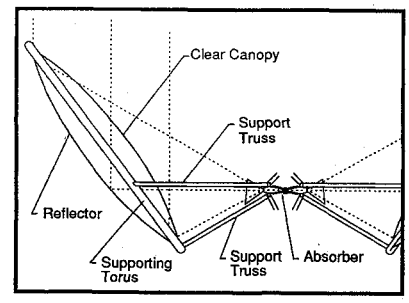

Fig. 1 Typical solar thermal design.

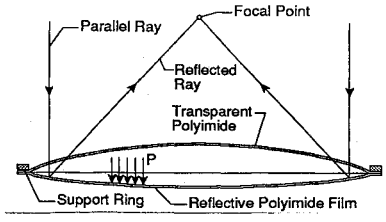

Fig. 2 Concept of a solar reflector.

the focal length must be known so that the greatest amount of energy may be collected. Prediction of the focal length and evaluation of the focus require that the effects of inflation pressures and heat transfer on the concentrator shell be known. To predict these effects, the material properties of the film must be known.

Previously available polyimides, such as Kapton, are only available in extruded flat films.[2] The only way that they may be formed into the parabolic shape required to concentrate solar energy is by heat relaxation, which causes the material properties of the film to change and therefore to be unpredictable, or by gore segment layup, which introduces seams in the film material. These seams have different material properties than the rest of the reflector structure. Heat relaxation and gore segment layup introduce new design problems, in that the material properties of the reflector are different from the original properties of the film. New polyimide materials have recently been developed to avoid these problems. These new polyimides (6FDA+APB and BTDA+ODA) are castable and exhibit equivalent, and in some cases superior, material properties to other polyimides.[3] The advantage to using these new polyimides over other materials such as Kapton is based upon the fact that 6FDA+APB and BTDA+ODA are castable, which allows the film to be formed on complex curved surfaces and retain all of its original material properties. Another unique characteristic of 6FDA+APB and BTDA+ODA polyimides is that they may be precast in a parabolic shape and then attached to an inflatable torus and stowed for deployment from the payload shroud. The shape of the parabolic reflector is maintained after deployment by the supporting torus and an applied pressure (P) inside a clear canopy, as shown in Figs. 1 and 2.

The purpose of this research is to evaluate the properties of these castable polyimides and determine the effects of their properties on beam quality. Since the concentrator design must be validated in ground tests prior to flight, the material-property testing must permit determination of behavior on both ground and space-flight operation. For example, a ground test model is exposed to additional environmental conditions, such as humidity, which it will not experience in flight. Therefore, this study includes the hygroscopic effects of the film material. This study evaluates the two proposed polyimide materials that are to be used in the construction of a ground-test reflector.

Methods

Determination of Material Properties

The modulus of elasticity and coefficient of thermal expansion (CTE) of the 6FDA+APB polyimide were determined experimentally using a uniaxial test apparatus.[4] The uniaxial test apparatus was designed specifically for materials tests with thin-film materials approximately 0.0005 to 0.002 in. thick. The apparatus takes data through a linear-variable differential transformer (LVDT), which measures the displacement of the film, and a load cell, which measures the load applied to the film. The data are transferred to a computer through a signal conditioning system and a National Instruments data acquisition board. The data are recorded using LabVIEW™. LabVIEW uses a test panel that provides the user with film conditions such as applied load, displacement, and temperature. The entire test is monitored at this panel. The apparatus incorporates specially designed toggle grips at the ends of the load arms to grip the film. The grips apply a uniform, distributed load on the film to prevent stress concentrations. Load is provided by a stepper motor, which can be adjusted to various rates to provide constant uniform loading. The test setup also includes a temperature chamber, which is used in tests to determine thermal expansion coefficient, thermal stress relaxation, and thermal creep under an applied load.

All modulus-of-elasticity tests were performed at room temperature and repeated a number of times to establish a pattern. All the tests were performed on samples obtained from the same batch, but from two different castings having equivalent conditions. The device used to cut the film was designed to provide parallel cuts along the length of the test sample and to reduce the likelihood of small nicks in the film. After the samples were cut, their dimensions were recorded. The samples were then placed in the materials tester. Load

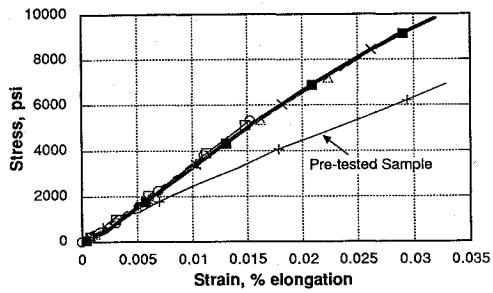

Fig. 3 Comparision of 6FDA+APB modulus data.

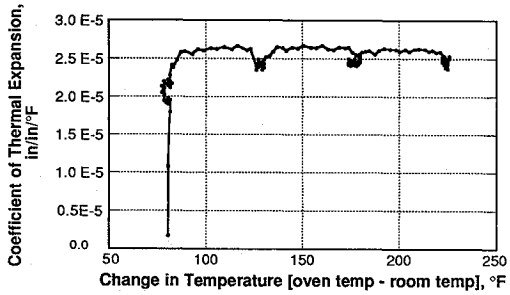

Fig. 4 CTE for 6FDA+APB polyimide.

was provided to the film at a constant rate through the linear motor, and the displacement of the film was recorded through the LVDT. The films were tested to failure to provide the most complete data.

The strain of the film was calculated from the displacement data and plotted against the stress, which was calculated from the applied-load data taken by the load cell. The modulus of elasticity was determined from the slope of the linear portion of the stress–strain diagram, taken by a linear curve fit on the computer. The results from the modulus tests for the 6FDA+APB polyimide experienced a 5% scatter. The trends of the 6FDA+APB polyimide tests, shown in Fig. 3, show the modulus of elasticity to be constant with every trial with the exception of the pretested sample. The latter would not be expected to follow the trend, because it had been loaded beyond its elastic limit in a previous test. This pretested sample exemplifies the discussion made earlier about the formation of Kapton polyimides into complex curved shapes. In order to form Kapton or other flat films, they must be deformed by heat relaxation. Heat relaxation causes a permanent deformation in the film, which causes the material properties to change, as shown with the pretested sample above. This change makes the material properties difficult to predict and serves as an additional motivation to use the castable polyimides discussed in this paper.

The CTE was determined for the 6FDA+APB polyimides over a range of temperatures. This range, room temperature to 300°F, is important because it is the temperature range at which the film is cured and to which it is most likely to be exposed during normal applications.

Samples of the 6FDA+APB polyimide were cut from the same castings as the samples for the modulus tests. Their dimensions were recorded, and they were mounted in the materials tester. The temperature chamber was raised to the first test temperature and allowed to stabilize for a period of 3 h. The data acquisition system was started, and the film was moved into the chamber. The displacement of the film was measured, and the temperature was raised. The strain in the film at the five temperatures was calculated. The CTE of the polyimide was determined by dividing the changes in strain by the changes in temperature. The CTE of the 6FDA+APB polyimide, shown in Fig. 4, was linear over the range of temperatures tested. The deviations in the CTE curve are transition points in the oven temperature.

The material tests performed on these films conform to ASTM standards. Their results were compared with data provided by the supplier of the film,[5,6] as shown in Table 1, to verify the accuracy of the data. Additional tests were not performed on the BTDA+ODA because of the low percentage difference found in the 6FDA+APB

Table 1 Experimental material properties

	Modulus, psi	CTE, in./(in. °F)
Experimental	457,500	25.7E–6
Manufacturer's	452,000	27.2E–6
Difference, %	1.3	5.7

tests. The data provided for the BTDA+ODA polyimide were taken to be reliable.

Parametric Analysis Code

A computer code has been developed to predict the deflections in a thin-film membrane.[7] The parametric analysis code used in this study is based upon closed-form mathematical theory that describes a symmetrically loaded shell of revolution.[8] This theory includes spherical and parabolic shapes. The solution is refined to include thermal and hygroscopic effects and linear variations in film thickness.

To determine the displacements, the analytical model uses membrane theory where no bending forces are included. The membrane is also axisymmetrically loaded with no shearing stresses. These assumptions for the stress conditions of the membrane are valid for a thin parabolic membrane toward the center portion away from the edge. Additional assumptions made in the development of the code include uniform temperature and humidity across the membrane.

The code uses a Romberg numerical integration routine to solve for the membrane displacement solution. The integration program was used as a subroutine for a series of computer programs written to determine the displacements of the membrane shapes. Newton–Cotes integration formulas are used, which pass a polynomial through points of the function and then integrate the polynomial approximation of the function. This computer code generates a set of data points that describe the deflected shape of a parabolic membrane. The data are transferred to an optical ray-trace code for the final focal-point prediction.[7]

Optical Ray-Trace Code

The deflections generated by the parametric analysis code describe the deformed shape of the membrane. Although these deflections may be useful during the fabrication of the membrane itself, they do not provide much information that would be considered useful to the designer of a solar rocket engine. The engine designer needs to know the effects of the deflections on the beam characteristics at the focal plane. An optical ray-trace code was used to generate this information.

BEAM 4 is an optical ray-trace tool capable of providing an easy means of exploring the properties of an optical system.[9] The ray-trace code is designed to be used to study a variety of optical needs, including 1) pilot designs of concentrators, camera lenses, telescopes, and collimators, 2) production of spot diagrams for illuminators or complete image-forming systems, 3) graphs illustrating system performance, and 4) tolerance analysis for focus dispersion, tilt, decenter, curvature, polynomial profile, and axial location error.

In this study, BEAM 4 was used to analyze the concentrator's optical properties. It first provides a curve fit to the points described by the parameter code. This curve fit describes the reflective portion of the concentrator. Rays are bounced off of this curve and converge at a focal point. The ray-trace code locates the point at which the concentration of the rays is the highest. This point is defined as the optimum focal point (f_o). BEAM 4 is also used to determine the distribution of rays at a fixed focal length (f) of 120 in. This is done to exhibit the importance of determining the optimum focal point for a concentrator setup to be designed where the focal point is fixed.

The rays incident on the concentrator in this analysis were assumed to be at 90 deg to the aperture. The sun's actual rays have a 1/2-deg divergence. Therefore, the values for the dispersions and focal-length increases presented in this study are not exact. However, the trends shown for the focal-point dispersion and focal-length increase are the same. BEAM 4 assumes 100% reflectivity for mirrors. It is not possible to allow for the actual reflectivity, which is approximately 90%, of the concentrators studied with this tool. The values presented here are only approximations to the actual energy that would be reflected from a real-life model.

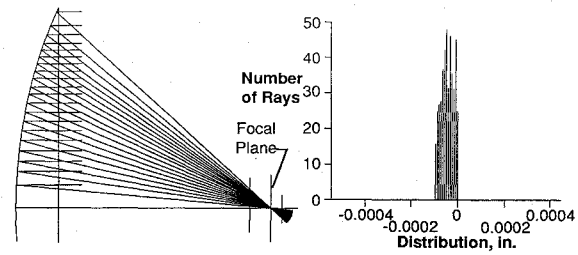

Fig. 5 Ray trace of undeformed membrane.

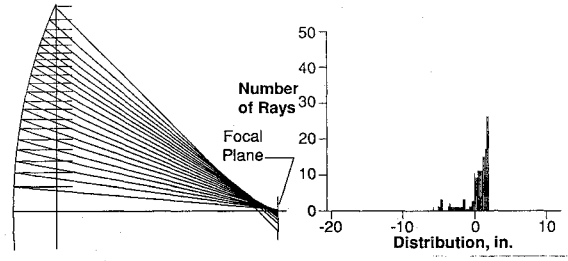

Fig. 6 Ray trace of membrane deformed by pressure.

Ray traces for representative cases are shown. A sample ray trace of the undeformed mirror from case BASELINE is shown in Fig. 5. The focal-point distribution is shown to be approximately 0.0001 in. at the optimum focal plane located at 120 in. from the vertex of the mirror. A sample ray trace of a deformed reflector is shown in Fig. 6, where the distribution at the location of the optimum focal point is approximately 8 in. Note the dispersed rays at the focal plane of the mirror.

Experimental Procedure

A parametric analysis was performed to determine the effects of the varied conditions (P, ΔT, ΔRH, and film thickness) upon two polyimide films. A test matrix, shown in Table 2, was generated which allowed systematic variation of the parameters. The effects of each condition on each film was examined individually and in combination with other conditions. The effects were determined by the parametric analysis code in the form of deflections from the original shape of the reflector. A total of 17 cases were run. For each case, the deflection from the original shape was determined and imported into the ray-trace code to determine the focal-point dispersion and translation.

The steps followed in this analysis are as follows. First, the material properties for both polyimide materials were determined. Table 3 shows the properties of the materials evaluated in this study. Some of these properties were determined experimentally,[4] and others were provided by the manufacturer.[5,6] Data for Poisson's ratio were not available. Previous studies[10,11] state that Poisson's ratio for thin-film polyimides varies between 0.34 and 0.48. The extremes of this range for polyimide materials were used to determine the maximum effects of this parameter. The applied conditions used in this study are representative of the expected conditions to which a typical laboratory model is exposed. The pressure was varied at levels that resulted in membrane stresses ranging from 300 to 2500 psi. The temperature and relative humidity were varied by 50 deg and 50%, respectively. These values are more than generous for the expected conditions which will be applied to the laboratory model.

After the test matrix was generated and the material properties had been determined, the case studies were run. For each case the first step was to input the material properties, film thickness, and application conditions into the parametric analysis code, which provided a set of data points that described the deformed shape of the concentrator. The deformed shape was then imported into the BEAM 4 code so that the optical analysis of the reflector could be done. The first step in the optical analysis involved optimizing the deformed shape of the concentrator. BEAM 4 allows a sixth-order curve fit. Typical rms values for a curve fit of the optimized shape were on the order of 0.0001–0.003.

Table 2 Parametric analysis test matrix

Test name	E	ν	CTE	CME	T_i	T_f	P	ΔT	ΔRH	Parameter varied from case A
BASELINE	N/A	N/A	N/A	N/A	0.001	0.001	N/A	N/A	N/A	
6FDA+APB										
Case 1A	457.5E3	0.34	25.7E−6	4.3E−6	0.001	0.001	0.005	0.0	0.0	
Case 1B	457.5E3	0.34	25.7E−6	4.3E−6	0.001	0.001	0.015	0.0	0.0	Pressure
Case 1C	457.5E3	0.34	25.7E−6	4.3E−6	0.001	0.002	0.005	0.0	0.0	Film thickness
Case 1D	457.5E3	0.34	25.7E−6	4.3E−6	0.001	0.001	0.005	50.0	0.0	Temperature
Case 1E	457.5E3	0.34	25.7E−6	4.3E−6	0.001	0.001	0.005	0.0	50.0	Humidity
Case 1F	457.5E3	0.48	25.7E−6	4.3E−6	0.001	0.001	0.005	0.0	0.0	Poisson's ratio
Case 1G	457.5E3	0.34	25.7E−6	4.3E−6	0.001	0.001	0.015	50.0	50.0	Pressure, temp., humidity
Case 1H	457.5E3	0.34	25.7E−6	4.3E−6	0.001	0.0015	0.005	0.0	0.0	Film thickness
Case 1I	457.5E3	0.34	25.7E−6	4.3E−6	0.001	0.00125	0.005	0.0	0.0	Film thickness
Case 1J	457.5E3	0.34	25.7E−6	4.3E−6	0.001	0.0015	0.015	0.0	0.0	Film thickness, pressure
Case 1K	457.5E3	0.34	25.7E−6	4.3E−6	0.001	0.00125	0.015	0.0	0.0	Film thickness, pressure
BTDA+ODA										
Case 2A	432.6E3	0.34	15.6E−6	28.5E−6	0.001	0.001	0.005	0.0	0.0	
Case 2B	432.6E3	0.34	15.6E−6	28.5E−6	0.001	0.001	0.015	0.0	0.0	Pressure
Case 2C	432.6E3	0.34	15.6E−6	28.5E−6	0.001	0.002	0.005	0.0	0.0	Film thickness
Case 2D	432.6E3	0.34	15.6E−6	28.5E−6	0.001	0.001	0.005	50.0	0.0	Temperature
Case 2E	432.6E3	0.34	15.6E−6	28.5E−6	0.001	0.001	0.005	0.0	50.0	Humidity
Case 2F	432.6E3	0.48	15.6E−6	28.5E−6	0.001	0.001	0.005	0.0	0.0	Poisson's ratio

Table 3 Material properties used in analysis

	6FDA+APB	BTDA+ODA
Modulus, psi	457,500	432,600
CTE, in./(in. °F)	25.7E−6	15.6E−6
CME, in./(in. %)	4.3E−6	28.5E−6
Poission's ratio, in./in.	0.34,0.48	0.34,0.48

When the shape of the reflector had been fitted, the optimum focal length was determined. The optimum focal length f_o is defined as the distance from the vertex of the mirror at which the focal-point dispersion is minimum. Each case was evaluated at its optimum focal length and at a fixed focal length f of 120 in. The purpose of evaluating the concentrator at fixed focal length was to demonstrate the importance of this analysis. For instance, if a concentrator setup were designed to have a fixed focal length that could not be adjusted, this analysis would provide meaningful information about the location of the optimum focal length to get the maximum amount of energy from the concentrator, thereby increasing the efficiency of the system. Each case was treated as a separate concentrator. The test matrix allowed the systematic evaluation of the effects of the material properties; the results are discussed systematically in the following section.

Results

The importance of the prediction of the effects of differing material properties and various applied conditions becomes apparent when studying the results of this effort. It is shown that the effects of the applied conditions differ for each material. For example, the 6FDA+APB polyimide has a lower CME than that of the BTDA+ODA. Therefore, the effects of relative humidity may be minimized by choosing the 6FDA+APB to construct a ground test model.

These studies show that two things happen to the concentrator when subjected to the conditions studied. The focal length of the concentrator increases, and the focus becomes blurred. The increase in focal length may be explained by the deflection at the center of the concentrator. The concentrator, when subjected to these applied conditions, actually experiences a flattening effect.[7] This flattening causes the concentrator's focal length to increase. The observed defocusing at the focal point is caused by the deviation in shape from a perfect parabola as the concentrator flattens.

Table 4 contains the results of the analysis. The discussion in the remainder of this section will focus on the focal-point dispersion

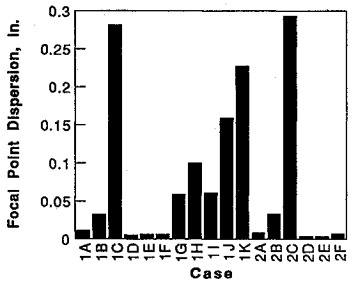

Fig. 7 Comparision of dispersions at f_o.

at the optimum focal point (f_o). As discussed earlier, the increase in focal length and dispersion at the fixed focal length f are only presented to give the reader a feel for what happens to the concentrator as various conditions are applied and to exhibit the importance of determining the optimum focal point so that the greatest possible energy may be collected from the concentrator. A comparison of the focal-point dispersions at the optimum focal length for each case is shown in Fig. 7. This representation quickly identifies pressure and film thickness as the most significant variables. The results of these parametric studies have been separated according to the independent variables so that the latter may be discussed individually.

Film-Thickness Effects

Variations in material film thickness had the greatest effect on the dispersion of the focus of the reflector. In both the 6FDA+APB and BTDA+ODA polyimides (shown in Table 5), the increase in the focal length f_L decreases as the thickness at the edge of the membrane (T_f) increases. For the 6FDA+APB, which is examined more closely, the rms dispersion at f_o increases as T_f increases. However, the rms dispersion at f decreases and then increases again at some thickness T_f greater than 0.0015 in. This indicates that there is an optimum T_f. For the cases studied, that thickness is 0.0015 in.

Pressure Effects

As shown in Table 6, the pressure was varied from 0.005 to 0.015 psi. The results of varied applied pressure show that the f_L increase, the rms dispersion at f, and the rms dispersion at f_o all increased approximately 300%. The fact that the increases were similar for the two materials is explained by their near-identical moduli of elasticity.

Table 4 Matrix of parametric analysis results

Test name	Offset	f	rms dispersion at fixed f	f_o	rms dispersion at optimum f_o	Focal-length increase	Parameter varied from case A
BASELINE	0.0	120.0	$-\infty$	120.0	$-\infty$	0.0	
6FDA+APB							
Case 1A	−0.2079	120.0	0.2970	120.6859	0.0110	0.6859	
Case 1B	−0.6236	120.0	0.8893	122.0560	0.0326	2.0560	Pressure
Case 1C	−0.1991	120.0	0.3050	120.2445	0.2811	0.2445	Film thickness
Case 1D	−0.5225	120.0	0.2579	120.9339	0.0050	0.9339	Temperature
Case 1E	−0.2605	120.0	0.2874	120.7185	0.0060	0.7185	Humidity
Case 1F	−0.1638	120.0	0.2770	120.6051	0.0060	0.6051	Poisson's ratio
Case 1G	−0.9909	120.0	0.8145	122.3005	0.0583	2.3005	Pressure, temp., humidity
Case 1H	−0.1994	120.0	0.1047	120.2482	0.1000	0.2482	Film thickness
Case 1I	−0.2056	120.0	0.1150	120.3602	0.0612	0.3602	Film thickness
Case 1J	−0.5621	120.0	0.1730	120.6736	0.1590	0.6736	Film thickness, pressure
Case 1K	−0.6168	120.0	0.4649	121.2650	0.2276	1.2650	Film thickness, pressure
BTDA+ODA							
Case 2A	−0.2198	120.0	0.3116	120.7164	0.0080	0.7164	
Case 2B	−0.6595	120.0	0.9395	122.1742	0.0330	2.1742	Pressure
Case 2C	−0.2106	120.0	0.3270	120.2636	0.2935	0.2636	Film thickness
Case 2D	−0.4108	120.0	0.2904	120.8733	0.0040	0.8733	Temperature
Case 2E	−0.5688	120.0	0.2723	121.0033	0.0035	1.0033	Humidity
Case 2F	−0.1732	120.0	0.2944	120.6421	0.0070	0.6421	Poisson's ratio

Table 5 Thickness effects

Case	Thickness T_f	f_L increase	rms dispersion f	rms dispersion f_o
1A	0.001	0.6859	0.2970	0.0110
1I	0.00125	0.3602	0.1150	0.0612
1H	0.0015	0.2482	0.1047	0.1000
1C	0.002	0.2445	0.3050	0.2811
2A	0.001	0.7164	0.3116	0.0080
2C	0.002	0.2636	0.3270	0.2935

Table 6 Pressure effects

Case	Pressure	f_L Increase	rms dispersion f	rms dispersion f_o
1A	0.005	0.6859	0.2970	0.0110
1B	0.015	2.0560	0.8893	0.0326
2A	0.005	0.7164	0.3116	0.0080
2B	0.015	2.1742	0.9395	0.0330

Table 7 Thickness and pressure effects[a]

Case	Thickness T_f	f_L increase	rms dispersion f	rms dispersion f_o
1B	0.001	2.0560	0.8893	0.0326
1K	0.00125	1.2650	0.4649	0.2276
1J	0.0015	0.6736	0.1730	0.1590

[a]Pressure = 0.015 psi.

Pressure and Thickness Effects

In this case (shown in Table 7) the thickness T_f was increased for the 6FDA+APB at a higher pressure. The data indicate that the f_L increase is reduced as T_f increases. The rms dispersion at f is reduced, but at f_o it increases and then is reduced as in the case at lower pressure. This again indicates that there is an optimum thickness T_f for the cases studied, and that thickness is 0.0015 in. Figure 8 is a plot of the effects of film thickness T_f on focal-point dispersion at the two pressures evaluated. It is interesting to note that the optimum thickness T_f is the same for both pressures. This is considered to be an important finding for the fabrication of a solar concentrator. As exhibited earlier in Fig. 7, the independent variables of temperature, humidity, and Poisson's ratio had little effect on focal-point dispersion compared to the effects of film thickness.

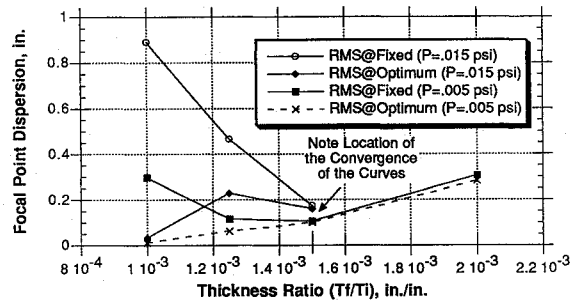

Fig. 8 Effects of varied film thickness at two different pressures.

Conclusions

With regard to fabrication techniques and cure cycles, it was determined that the 6FDA+APB polyimide would be the optimum choice for the material to be used in the construction of a ground test model or a flight article. Therefore it is discussed in the greatest detail.

It was found that, for the properties and conditions studied, a linear increase in film thickness with radius had the greatest effect upon energy dispersion at the focal plane for the concentrator geometry used. This is a significant finding, in that film thickness can be controlled during the fabrication process. Thus, this analysis may be used as a design tool in the construction of a solar concentrator. By varying the film thickness during fabrication, engineers may tune the concentrator to provide the optimum energy to the absorber of a solar thermal rocket engine.

Another useful finding is the effect of various material properties and operating conditions on the focal length of the reflector. Knowledge of the focal length of the concentrator allows the designer to construct its support structure in such a way that the solar rocket's absorber is at the optimum focal point of the reflector so that the greatest possible energy may be collected, thereby increasing the efficiency of the system.

The results of this study are considered to be reliable. The techniques outlined here provide a powerful tool in the design and fabrication of any reflector made from a thin membrane.

Acknowledgments

The research is currently being supported by the Air Force Phillips Laboratory, Edwards Air Force Base, California. The research was

performed at SRS Technologies, Huntsville, Alabama. Kristi K. Laug served as the Air Force's technical monitor.

References

[1]Clayton, W., and Gierow, P., "Inflatable Concentrators for Solar Thermal Propulsion," *Proceedings of the 1992 ASME–JSME International Energy Conference*, 1992.

[2]Downes, M., "Kapton Polyimide Material Properties," Product Summary Bulletin, Dupont Co., May 1983.

[3]St. Clair, A., St. Clair, T., and Shemp, W., "Optically Transparent/Colorless Polyimides," NASA TM 87650, Dec. 1985.

[4]Paxton, J., "Determination of Selected Material Properties of Castable Thin Film Polyimides for Applications in Solar Thermal Propulsion," *Proceedings of the 1994 AIAA Southeastern Regional Student Conference*, Huntsville, AL, 1994.

[5]Briggs, C., "Material Properties of 6FDA+APB Polyimide Films," private communication, June 1991.

[6]Gierow, P., and Moore, J., "Thin Film Creep-Forming for Solar Thermal Propulsion," Final Rept., Contract F04611-87-C-0065, June 1990.

[7]Gierow, P., "Prediction of the Response of a Parabolic Membrane," Master's Thesis, Univ. of Alabama in Huntsville, May 1994.

[8]Timoshenko, S. P., *Theory of Plates and Shells*, McGraw–Hill, New York, 1961.

[9]Lampton, M., *BEAM 4 Users Guide*, Stellar Software, Berkeley, CA, Jan. 1994.

[10]Bauer, C. L., and Farris, R. J., "Determination of Poisson's Ratio for Polyimide Films," *Polymer Eng. and Sci.*, Vol. 29, No. 16, 1989, pp. 1107–1110.

[11]Maden, M., "The Determination of Stress and Material Properties of Polyimide Coatings and Films Using Real Time Holographic Interferometry," Ph.D. Dissertation, Univ. of Massachusetts, May 1992.

H. R. Anderson
Associate Editor